[16] S. M. Rytov, "Electromagnetic properties of a finely stratified medium," *Sov. Phys. JETP,* vol. 2, p. 466, 1956.
[17] G. D. Mahan, "Long-wavelength absorption of cermets," *Phys. Rev. B,* vol. 38, p. 9500, 1988.
[18] O. Acher, J. L. Vermeulen, P. M. Jacquart, J. M. Fontaine, and P. Baclet, "Permeability measurement on ferromagnetic thin films from 50 MHz up to 18 GHz," *J. Magn. Mat.,* vol. 136, p. 269, 1994.

Dispersion Characteristics of Cylindrical Coplanar Waveguides

Hsin-Cheng Su and Kin-Lu Wong

***Abstract*— A full-wave analysis of the coplanar waveguide (CPW) printed on a cylindrical substrate is presented, and the dispersion characteristics of the cylindrical CPW are studied. Numerical results of the effective relative permittivity are calculated using a Galerkin's moment-method calculation. Experiment is also conducted, and the measured data are in good agreement with the theory.**

I. Introduction

Although coplanar waveguides (CPW's) provide some advantages over microstrip lines [1], such as easier connection with integrated active devices and no via holes for grounding, etc., it is noted that the studies of conformal CPW's receive much less attention than conformal microstrip lines. The microstrip lines mounted on curved surfaces, such as cylindrical [2], [3], or elliptical [4] bodies, have been extensively studied. However, to the best of our knowledge, the studies of conformal CPW's have not yet been reported in the open literature. To increase the application of CPW's on curved surfaces and analyze the dispersion characteristics of conformal CPW's, we present in this paper a full-wave analysis of the CPW printed on a cylindrical substrate. Numerical results of the frequency-dependent effective relative permittivity are calculated and analyzed. Measured data are also presented for comparison with the calculated results, and the curvature effect on the effective relative permittivity of the CPW is discussed.

II. Theoretical Formulation

Fig. 1 shows the geometry of a cylindrical coplanar waveguide. The CPW is assumed to be infinitely long, and the radius of the cylindrical ground plane is b. The thickness and relative permittivity of the substrate is $h(=b-a)$ and ε_2, respectively. The width of the signal strip is S, and the ground-to-ground spacing is d. The region $\rho < a$ is assumed to have a relative permittivity ε_1. Outside the ground plane is air with free-space permittivity ε_0 and permeability μ_0.

To begin with, the spectral-domain Helmholtz's equations in each region of the structure are solved, which gives the expressions of the spectral amplitudes of the electric and magnetic fields in inner region ($\rho < a$), substrate layer ($a \le \rho \le b$), and outer region ($\rho > b$). Then, by applying the equivalence principle [5], the slot region between the signal strip and the ground can be closed off and replaced by an equivalent magnetic surface current density $\vec{M}_s(= M_\phi\hat{\phi} + M_z\hat{z})$ at (b^-, ϕ, z) and $-\vec{M}_s$ at (b^+, ϕ, z). When imposing the boundary conditions of the structure and manipulating the derived field components, we can relate the difference of the tangential magnetic fields at $\rho = b^-$ and $\rho = b^+$ to the magnetic surface current density as

$$\begin{bmatrix}\Delta\tilde{H}_\phi \\ \Delta\tilde{H}_z\end{bmatrix} = [\overline{\overline{G}}^{(s)} - \overline{\overline{G}}^{(a)}] \cdot \begin{bmatrix}\tilde{M}_\phi \\ \tilde{M}_z\end{bmatrix} = \begin{bmatrix}0 \\ 0\end{bmatrix} \tag{1}$$

where $\overline{\overline{G}}^{(s,a)} = \hat{\phi}\tilde{G}_{\phi\phi}^{HM^{(s,a)}}\hat{\phi} + \hat{\phi}\tilde{G}_{\phi z}^{HM^{(s,a)}}\hat{z} + \hat{z}\tilde{G}_{z\phi}^{HM^{(s,a)}}\hat{\phi} + \hat{z}\tilde{G}_{zz}^{HM^{(s,a)}}\hat{z}$ is dyadic Green's functions showing the H_ϕ or H_z fields on the substrate (s) or air (a) sides of the slot region due to a unit M_ϕ or M_z at the slot region. The expressions of the Green's functions are derived in the Appendix, and the tilde denotes a Fourier transform. ΔH shows the difference of the tangential magnetic fields at $\rho = b^-$ and at $\rho = b^+$, which must be zero to satisfy the boundary condition that the continuity of the tangential magnetic fields at the slot region must hold.

And, due to the assumption that the cylindrical CPW is infinitely long, the magnetic surface current at the slot region can be assumed to have a traveling-wave form of $e^{j\beta z}$, where β is the effective propagation constant to be determined. In this case we have

$$\vec{M}_s = e^{j\beta z}[\hat{z}M_z(\phi) + \hat{\phi}M_\phi(\phi)]. \tag{2}$$

To apply the moment method, we choose N rooftop basis functions of the form

$$M_{\phi n} = 1 - \frac{2|\phi - \phi_{\phi n}|}{D_t}, \quad |\phi - \phi_{\phi n}| < \frac{D_t}{2} \tag{3}$$

with

$$\phi_{\phi n} = \frac{S}{2b} + \frac{nD_t}{2},$$
$$D_t = \frac{d-S}{b(N+1)}$$

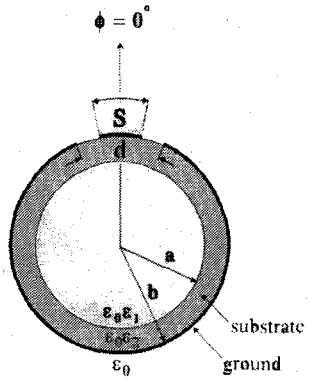

Fig. 1. The geometry of a cylindrical coplanar waveguide.

Manuscript received October 18, 1995; revised July 22, 1996. This work was supported by the National Science Council of the Republic of China under Grant NSC85-2221-E-110-002.

The authors are with the Department of Electrical Engineering, National Sun Yat-Sen University, Kaohsiung, Taiwan.

Publisher Item Identifier S 0018-9480(96)07904-5.

to expand $M_\phi(\phi)$, and M pulse basis functions of the form

$$M_{zm} = 1, \quad |\phi - \phi_{zm}| < \frac{D_z}{2} \tag{4}$$

with

$$\phi_{zm} = \frac{S}{2b} + \frac{(2m-1)D_z}{2}, \quad D_z = \frac{d-S}{2bM}$$

to expand $M_z(\phi)$. The selection of the basis functions of (3) and (4) makes the numerical computation efficient. And although they do not account for the edge effect, the propagation constants so calculated are within 1% of the results obtained from considering the edge effect [1]. It is also noted that since the ground planes on both sides of the signal strip are in contact and thus at the same potential (see Fig. 1), the excitation of the parasitic mode (even mode) [1] is suppressed. Thus, only the odd-mode propagation of the coplanar waveguide is considered here. In the odd-mode case, a magnetic wall at the center of the two slot regions can be assumed, which results in the odd-mode basis functions written as, in the spectral domain

$$\tilde{M}_{\phi n}^{(o)} = \frac{4}{\pi D_t p^2} \sin^2\left(\frac{pD_t}{4}\right) \cos(p\phi_{\phi n}) \tag{5}$$

$$\tilde{M}_{zm}^{(o)} = \frac{j}{p\pi} \sin\left(\frac{pD_z}{2}\right) \sin(p\phi_{zm}). \tag{6}$$

Using the above selected basis functions as testing functions and applying Galerkin's method to (1), we can have the following homogeneous matrix equation

$$\begin{bmatrix} (Y_{ln}^{\phi\phi})_{N\times N} & (Y_{lm}^{\phi z})_{N\times M} \\ (Y_{kn}^{z\phi})_{M\times N} & (Y_{km}^{zz})_{M\times M} \end{bmatrix} \begin{bmatrix} (I_{\phi n})_{N\times 1} \\ (I_{zm})_{M\times 1} \end{bmatrix} = \begin{bmatrix} 0 \\ 0 \end{bmatrix} \tag{7}$$

where

$$Y_{ln}^{\phi\phi} = \sum_{p=-\infty}^{\infty} \tilde{M}_{\phi l}^{(o)}(-p)[\tilde{G}_{\phi\phi}^{HM^{(s)}}(b, p, \beta) - \tilde{G}_{\phi\phi}^{HM^{(a)}}(b, p, \beta)]\tilde{M}_{\phi n}^{(o)}(p), \tag{8a}$$

$$Y_{lm}^{\phi z} = \sum_{p=-\infty}^{\infty} \tilde{M}_{\phi l}^{(o)}(-p)[\tilde{G}_{\phi z}^{HM^{(s)}}(b, p, \beta) - \tilde{G}_{\phi z}^{HM^{(a)}}(b, p, \beta)]\tilde{M}_{zm}^{(o)}(p), \tag{8b}$$

$$Y_{kn}^{z\phi} = \sum_{p=-\infty}^{\infty} \tilde{M}_{zk}^{(o)}(-p)[\tilde{G}_{z\phi}^{HM^{(s)}}(b, p, \beta) - \tilde{G}_{z\phi}^{HM^{(a)}}(b, p, \beta)]\tilde{M}_{\phi n}^{(o)}(p), \tag{8c}$$

$$Y_{km}^{zz} = \sum_{p=-\infty}^{\infty} \tilde{M}_{zk}^{(o)}(-p)[\tilde{G}_{zz}^{HM^{(s)}}(b, p, \beta) - \tilde{G}_{zz}^{HM^{(a)}}(b, p, \beta)]\tilde{M}_{zm}^{(o)}(p) \tag{8d}$$

$$l, n = 1, 2, \cdots, N,$$
$$k, m = 1, 2, \cdots, M.$$

In (7), $I_{\phi n}$ and I_{zm} are unknown coefficients for the magnetic surface current. To have nontrivial solutions for $I_{\phi n}$ and I_{zm}, the determinant of (7) must vanish, i.e.,

$$\det \begin{bmatrix} (Y_{ln}^{\phi\phi})_{N\times N} & (Y_{lm}^{\phi z})_{N\times M} \\ (Y_{kn}^{z\phi})_{M\times N} & (Y_{km}^{zz})_{M\times M} \end{bmatrix} = 0. \tag{9}$$

From solving (9), the effective propagation constant β of the cylindrical CPW is obtained, and the effective relative permittivity ε_{eff} can be calculated from $(\beta/k_0)^2$.

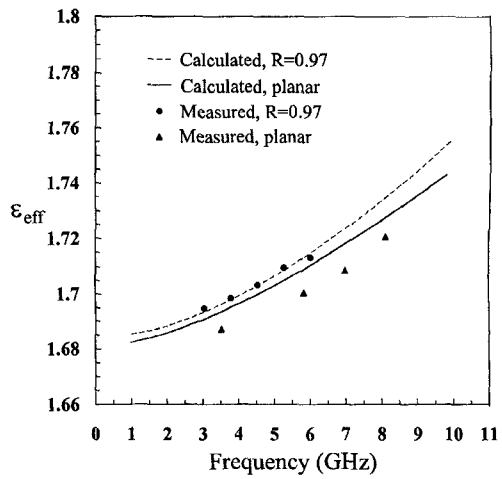

Fig. 2. Effective relative permittivity versus frequency; $\varepsilon_1 = 1.0$, $\varepsilon_2 = 3.0$, $h = 1.524$ mm, $d = 7$ mm, and $S/d = 0.572$. The theoretical results for the planar CPW are calculated using a full-wave approach described in [1].

III. Results and Discussion

Fig. 2 shows the effective relative permittivity versus frequency. The region $\rho < a$ is here assumed to be air. The curvature of the cylindrical CPW is defined using a curvilinear coefficient $R(= a/b)$, the ratio of inner to outer radii [2] and [3]. In the numerical calculation, a total of six ($N = M = 3$) basis functions is used, which shows good numerical convergence. The theoretical results for the planar CPW are calculated using a full-wave approach described in [1]. Both the planar CPW and the cylindrical CPW with $R = 0.97$ were constructed using flexible copper-clad microwave substrate RO3003, a ceramic filled PTFE composite whose dielectric constant versus temperature is very stable. Two types of the cylindrical CPW were constructed: one was constructed exactly as the geometry shown in Fig. 1, and the other was constructed with only half the circumference of the ground cylinder (the two ground planes on both sides of the signal strip were connected to be at the same potential). The measurement was performed using an HP8510C network analyzer, and the measurement error in this study was estimated to be within 0.2%. No discrepancies between the measured data of the two types of cylindrical CPW's are seen, and the measured data are shown in Fig. 2 for comparison with the theoretical results. It is seen that the experiment is in good agreement with the theory. Results also indicate that the cylindrical CPW has a larger effective relative permittivity than the planar CPW.

Fig. 3 presents the effective relative permittivity versus frequency for different substrate thicknesses and curvilinear coefficients. It seems that the curvature effect on the effective relative permittivity is greater for a smaller substrate thickness, and however, the variation of the effective relative permittivity with frequency is greater for a larger substrate thickness. In Fig. 4, we present the effective relative permittivity versus normalized CPW size. It is found that the curvature effect becomes more significant when the CPW size increases.

IV. Conclusion

Dispersion characteristics of a cylindrical CPW have been studied using a full-wave formulation and a moment-method calculation. Theoretical results have been checked with the experiment, and good agreement is observed. Results also show that the effective relative permittivity of the CPW varies greatly with the curvature variation, and the variation is more significant for a larger CPW size.

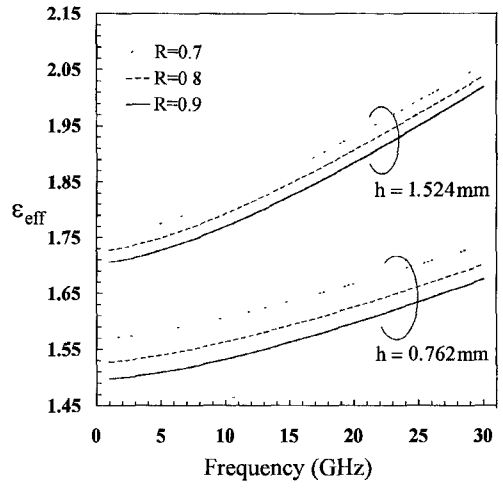

Fig. 3. Effective relative permittivity versus frequency with substrate thickness h and curvilinear coefficient R as parameters; $\varepsilon_1 = 1.0$, $\varepsilon_2 = 3.0$, $d = 7$ mm, and $S/d = 0.572$.

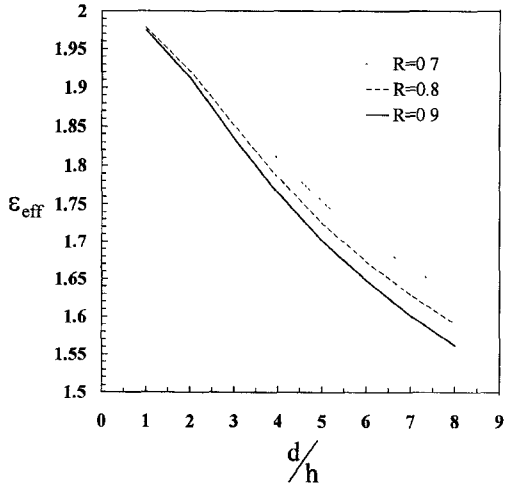

Fig. 4. Effective relative permittivity versus normalized CPW size (ground-to-ground spacing) with curvilinear coefficient R as parameters; $\varepsilon_1 = 1.0$, $\varepsilon_2 = 3.0$, $h = 0.762$ mm, $S/d = 0.5$, and $f = 10$ GHz.

APPENDIX

The components of the dyadic Green's functions in (1) are derived as (in the spectral domain)

$$\tilde{G}_{\phi\phi}^{HM^{(s)}}(b, n, k_z) = \frac{-j4\omega\varepsilon_0}{X_n\pi^2 k_{\rho2}^4 T_b ab}\left\{\frac{\varepsilon_2}{T_a}\left[\frac{n^2k_z^2}{k_{\rho2}ab}\left(\frac{1}{k_{\rho1}^2}-\frac{1}{k_{\rho2}^2}\right) - \frac{\varepsilon_2 T_b k_0^2}{T_a}\left(\frac{\alpha_n}{k_{\rho1}}-\frac{T_d}{k_{\rho2}T_b}\right)\right] + \frac{n^2 D_n k_z^2}{k_{\rho2}bT_b}\right\} + \frac{j\omega\varepsilon_0}{k_{\rho2}}\left(\frac{\varepsilon_2 T_b}{T_a} - \frac{n^2k_z^2T_a}{k_0^2k_{\rho2}^2b^2T_b}\right),$$

$$\tilde{G}_{\phi\phi}^{HM^{(a)}}(b, n, k_z) = \frac{j\omega\varepsilon_0 n^2k_z^2\gamma_n}{k_0^2k_{\rho3}^3b^2} - \frac{j\omega\varepsilon_0}{\gamma_n k_{\rho3}},$$

$$\tilde{G}_{\phi z}^{HM^{(s)}}(b, n, k_z) = \frac{-j4\omega\varepsilon_0 nk_z}{X_n\pi^2k_{\rho2}^3T_aT_ba^2b}\cdot\left[\frac{\varepsilon_2}{k_{\rho2}^2}\left(1-\frac{aT_c}{bT_b}\right)+\frac{1}{k_{\rho1}}\left(\frac{\varepsilon_1\alpha_n aT_a}{k_{\rho2}bT_b}-\frac{\varepsilon_2}{k_{\rho1}}\right)\right] + \frac{j\omega\varepsilon_0 nk_zT_a}{k_0^2k_{\rho2}bT_b},$$

$$\tilde{G}_{\phi z}^{HM^{(a)}}(b, n, k_z) = -\frac{j\omega\varepsilon_0 nk_z\gamma_n}{k_0^2k_{\rho3}b},$$

$$\tilde{G}_{z\phi}^{HM^{(s)}}(b, n, k_z) = \tilde{G}_{\phi z}^{HM^{(s)}}(b, n, k_z),$$

$$\tilde{G}_{z\phi}^{HM^{(a)}}(b, n, k_z) = \tilde{G}_{\phi z}^{HM^{(a)}}(b, n, k_z),$$

$$\tilde{G}_{zz}^{HM^{(s)}}(b, n, k_z) = \frac{j4\omega\varepsilon_0}{X_n\pi^2k_{\rho2}^2T_b^2ab}\left(\frac{\varepsilon_1\alpha_n}{k_{\rho1}}-\frac{\varepsilon_2T_c}{k_{\rho2}T_a}\right) - \frac{j\omega\varepsilon_0k_{\rho2}T_a}{k_0^2T_b},$$

$$\tilde{G}_{zz}^{HM^{(a)}}(b, n, k_z) = \frac{j\omega\varepsilon_0\gamma_nk_{\rho3}}{k_0^2},$$

where

$$D_n = \frac{\varepsilon_2T_b}{aT_a}\left(\frac{1}{k_{\rho1}^2}-\frac{1}{k_{\rho2}^2}\right)+\frac{1}{k_{\rho2}b}\left(\frac{\varepsilon_2T_c}{k_{\rho2}T_a}-\frac{\varepsilon_1\alpha_n}{k_{\rho1}}\right),$$

$$T_a = J_n(k_{\rho2}b)H_n^{(1)}(k_{\rho2}a) - J_n(k_{\rho2}a)H_n^{(1)}(k_{\rho2}b),$$

$$T_b = J_n(k_{\rho2}a)H_n^{(1)\prime}(k_{\rho2}b) - J_n'(k_{\rho2}b)H_n^{(1)}(k_{\rho2}a),$$

$$T_c = J_n(k_{\rho2}b)H_n^{(1)\prime}(k_{\rho2}a) - J_n'(k_{\rho2}a)H_n^{(1)}(k_{\rho2}b),$$

$$T_d = J_n'(k_{\rho2}a)H_n^{(1)\prime}(k_{\rho2}b) - J_n'(k_{\rho2}b)H_n^{(1)\prime}(k_{\rho2}a),$$

$$X_n = \frac{n^2k_z^2}{a^2}\left(\frac{1}{k_{\rho1}^2}-\frac{1}{k_{\rho2}^2}\right) + k_0^2\left(\frac{\alpha_n}{k_{\rho1}}-\frac{T_d}{k_{\rho2}T_b}\right)\left(\frac{\varepsilon_2T_c}{k_{\rho2}T_a}-\frac{\varepsilon_1\alpha_n}{k_{\rho1}}\right),$$

$$\alpha_n = \frac{J_n'(k_{\rho1}a)}{J_n(k_{\rho1}a)},$$

$$\gamma_n = \frac{H_n^{(1)}(k_{\rho3}b)}{H_n^{(1)\prime}(k_{\rho3}b)}.$$

REFERENCES

[1] R. W. Jackson, "Considerations in the use of coplanar waveguide for millimeter-wave integrated circuits," *IEEE Trans. Microwave Theory Tech.*, vol. 34, pp. 1450–1456, Dec. 1986.

[2] N. G. Alexopoulos and A. Nakatani, "Cylindrical substrate microstrip line characterization," *IEEE Trans. Microwave Theory Tech.*, vol. 35, pp. 843–849, Sept. 1987.

[3] R. B. Tsai and K. L. Wong, "Characterization of cylindrical microstriplines mounted inside a ground cylindrical surface," *IEEE Trans. Microwave Theory Tech.*, vol. 43, pp. 1607–1610, July 1995.

[4] L. R. Zeng and Y. Wang, "Accurate solutions of elliptical and cylindrical striplines and microstrip lines," *IEEE Trans. Microwave Theory Tech.*, vol. 34, pp. 259–264, 1986.

[5] R. F. Harrington, *Time-Harmonic Electromagnetic Fields.* New York: McGraw-Hill, 1993, p. 106.